NANO LETTERS

2007
Vol. 7, No. 7
1960−1966

Influence of Structural and Dielectric Anisotropy on the Dielectrophoresis of Single-Walled Carbon Nanotubes

Sabine Blatt,*,† Frank Hennrich,† Hilbert v. Löhneysen,‡,§ Manfred M. Kappes,†,|| Aravind Vijayaraghavan,† and Ralph Krupke*,†,‡

Institut für Nanotechnologie, Forschungszentrum Karlsruhe, D-76021 Karlsruhe, Germany, Physikalisches Institut, Universität Karlsruhe, D-76128 Karlsruhe, Germany, Institut für Festkörperphysik, Forschungszentrum Karlsruhe, D-76021 Karlsruhe, Germany, and Institut für Physikalische Chemie, Universität Karlsruhe, D-76128 Karlsruhe, Germany

Received March 22, 2007; Revised Manuscript Received May 8, 2007

ABSTRACT

We report on a carbon nanotube network which is composed of aligned metallic and randomly oriented semiconducting single-walled carbon nanotubes. The material is formed by using a novel radio frequency dielectrophoresis setup, which generates very large dielectrophoretic force fields and allows dielectrophoretic assembling of nanotube films up to 100 nm thickness. Polarization dependent absorption measurements provide experimental evidence for the electronic type specific alignment behavior. We explain the experimental data with an advanced model for nanotube dielectrophoresis, which explicitly takes into account both the longitudinal and transversal polarizability. On the basis of this model, we calculate the dielectrophoretic force fields and show that semiconducting nanotubes deposit under very large fields due to their transversal polarizability even for high field frequencies.

The behavior of single-walled carbon nanotubes (SWNTs) under dielectrophoresis (DEP), i.e. the translational force and the torque exerted on suspended polarizable particles by an inhomogeneous electric field,[1] has attracted much attention recently. Apart from using DEP for the assembly of nanotubes and nanowires in a controlled way,[2−5] it was proven to be an effective method to separate metallic and semiconducting SWNTs.[6−11] So far in the numerical analysis of dielectrophoretic response, the dielectric anisotropy of carbon nanotubes was neglected and only polarization along the tube axis was taken into account.[12]

In this work, we discuss the influence of structural and dielectric anisotropy in the presence of very large electric fields. We propose an extended model of SWNT dielectrophoresis, which predicts effects like the deposition of semiconducting nanotubes for frequencies above the crossover frequencies measured before[7] and a severe difference in the alignment of metallic vs semiconducting nanotubes. Experimental evidence for the different alignment is provided in the form of polarization dependent absorption measurements on 60-nm thick films of SWNTs, which were deposited with a field strength of the order of 2×10^7 V/m onto an array of interdigitated electrodes. The orientation of the two nanotube types differs significantly: metallic nanotubes show a high degree of alignment parallel to the electric field lines, while semiconducting nanotubes are randomly oriented. In addition, finite element simulations are presented, that predict attractive forces acting on semiconducting nanotubes solely due to their perpendicular polarization.

The origin of the dielectrophoretic force and torque acting on a dielectric particle (with permittivity ϵ_2 and conductivity σ_2), which is suspended in a medium with different dielectric properties (ϵ_1,σ_1) and exposed to an inhomogeneous electric field $\boldsymbol{E}_{\text{ext}} = \boldsymbol{E}_0\,\text{Re}[\exp(i\omega t)]$, is the interaction of the particle's induced multipolar moments with the electric field.[1] Except for the case where the particle is located near zero field, the dielectric force and torque are well described within the effective-moment method, considering only the dipole moment $\boldsymbol{p}_{\text{eff}}$.[13] In this approximation the particle is assumed to be small compared to the characteristic length scale of the electric field and changes in the surrounding field due to the presence of the particle are neglected.[14] On the basis of the potential energy for an induced dipole, $U = -(1/2)\boldsymbol{p}_{\text{eff}}\cdot\boldsymbol{E}_{\text{ext}}$,[15] and using the appropriate form of the effective dipole, we can easily derive the force $\boldsymbol{F}_{\text{DEP}} = -\nabla U = (1/2)\nabla(\boldsymbol{p}_{\text{eff}}\cdot$

* Corresponding authors. E-mail: (S.B.) blatt@int.fzk.de; (R.K.) krupke@int.fzk.de.
† Institut für Nanotechnologie, Forschungszentrum Karlsruhe.
‡ Physikalisches Institut, Universität Karlsruhe.
§ Institut für Festkörperphysik, Forschungszentrum Karlsruhe.
|| Institut für Physikalische Chemie, Universität Karlsruhe.

10.1021/nl0706751 CCC: $37.00
Published on Web 06/19/2007

$\boldsymbol{E}_{\text{ext}}$) and torque $\boldsymbol{T}_{\text{DEP}} = \boldsymbol{p}_{\text{eff}} \times \boldsymbol{E}_{\text{ext}}$. In the case of alternating fields with sufficiently high frequencies, it is common practice to use the time averaged values $\langle \boldsymbol{F}_{\text{DEP}} \rangle$ and $\langle \boldsymbol{T}_{\text{DEP}} \rangle$.

The effective dipole moment $\boldsymbol{p}_{\text{eff}}$ can be expressed in terms of the particle volume and the effective polarizability tensor $\bar{\alpha}$ multiplied by the external field $\boldsymbol{E}_{\text{ext}}$. For spherical particles $\bar{\alpha}$ is a scalar multiple of the unitary matrix and $\boldsymbol{p}_{\text{eff}}$ is parallel to the electric field. The effective dipole moment of nonspherical particles on the other hand is different along each principal axis and therefore depends on the orientation of the particle with respect to the external field, particularly for anisotropic polarizability. We approximate a nanotube by an ellipsoid, which is analytically describable. When the anisotropy in the polarizability follows the principal axes, the dipole moment in the particle's coordinate system is given by $p_{\text{eff,n}} = \sum_{\text{m}} \alpha_{\text{nm}} \cdot E_{\text{ext,m}}$ for n, m = 1, 2, 3, where $\bar{\alpha}$ is a diagonal matrix with $\alpha_{\text{nn}} = 4/3\ \pi abc \epsilon_1 \text{Re}([\epsilon^*_{2,\text{n}} - \epsilon^*_1]/[\epsilon^*_1 + (\epsilon^*_{2,\text{n}} - \epsilon^*_1)L_{\text{n}}])$, n = 1, 2, 3.[14]

Here a, b, and c are the semi−major axes of the particle, L_{n} are the depolarization factors along the principal axes and $\epsilon^*_{1/2} = \epsilon_{1/2} - i\sigma_{1/2}/\omega$. Furthermore, we account for a dielectric anisotropy in the dielectric function of the particle, $\epsilon^*_{2,\text{n}}$. To determine the effective dipole moment and the dielectrophoretic force in the global coordinate system, a coordinate transformation is necessary: $\tilde{\alpha} = \boldsymbol{R}\bar{\alpha}\boldsymbol{R}^T$.[16]

The time averaged dielectrophoretic torque on ellipsoidal particles then has the following form: $\langle \boldsymbol{T} \rangle_{\text{k}} = {}^1/_2 E_{0,\text{m}} E_{0,\text{n}} [\alpha_{\text{mm}} - \alpha_{\text{nn}}] \delta_{\text{k,n,m}}$,[14] where $\delta_{\text{k,n,m}}$ is the Levi-Cevita tensor for $k, n, m = 1, 2, 3$ in the particle's coordinate system. The orientation of a lossless particle is stable, when its longest axis is aligned parallel to the external field. For lossy particles the stable orientation depends on the field frequency and abrupt changes from one stable orientation into another can be observed. This can be explained by the fact that a distinct relaxation time of the Maxwell−Wagner polarization exists for each of the principal axis. These relaxation times and the corresponding critical frequencies are defined as[14]

$$\nu^{\text{MW}}_{\text{n}} = [2\pi(\tau^{\text{MW}})_{\text{n}}]^{-1} = [(1 - L_{\text{n}})\sigma_1 - L_{\text{n}}\sigma_{2,\text{n}}]/[2\pi((1 - L_{\text{n}})\epsilon_1 - L_{\text{n}}\epsilon_{2,\text{n}})]$$

The same behavior is expected for lossless particles with surface induced conductivity.

SWNTs are rod-like particles with a length much larger than their diameter. Due to the rotational symmetry the particle properties can be described by their components parallel and orthogonal to the nanotube axis. If we approximate the SWNT shape by a prolate ellipsoid and choose the 1-axis of the particle's coordinate system parallel to the nanotube axis, it follows that $\alpha_{\text{para}} \equiv \alpha_{11}$ and $\alpha_{\text{ortho}} \equiv \alpha_{22} = \alpha_{33}$ with $L_{\text{para}} \approx 10^{-5}$ and $L_{\text{ortho}} = (1/2)(1 - L_{\text{para}})$. According to theoretical predictions SWNTs have highly anisotropic permittivities.[17,18] In the case of metallic nanotubes $\epsilon^{\text{met}}_{\text{para}} \gg \epsilon^{\text{met}}_{\text{ortho}}$, while for semiconducting nanotubes $\epsilon^{\text{semi}}_{\text{para}} \approx \epsilon^{\text{semi}}_{\text{ortho}} \approx \epsilon^{\text{met}}_{\text{ortho}}$ (here $\epsilon^{\text{met,semi}}_{\text{para}}$ corresponds to the above-defined $\epsilon_{2,1}$ and $\epsilon^{\text{met,semi}}_{\text{ortho}}$ corresponds to $\epsilon_{2,2}$). In previous work we have argued that the conductivity of micellated semiconducting nanotubes is dominated by surface conductivity rather than the intrinsic conductivity.[7] Also, the DEP forces acting on metallic SWNTs in the low-frequency regime are comparable to those acting on semiconducting SWNTs, indicating a similar value of the conductivity. Therefore, we assume an equal and isotropic value of σ_2 for both nanotube types. The rotational energy for an individual SWNT is given by

$$U_{\text{ROT}} = \int \langle \boldsymbol{T} \rangle \, \text{d}\varphi = -1/4\ E_0{}^2 [\alpha_{\text{para}} - \alpha_{\text{ortho}}] \cos^2 \varphi \equiv U_0 \cos^2 \varphi$$

where the angle between the long axis and the electric field is denoted by φ.

During a dielectrophoretic deposition experiment both translational and rotational movement activated by the dielectrophoretic force and torque respectively are opposed by the random Brownian motion of the nanotubes due to their thermal energy. Therefore, the degree of alignment of the nanotubes in suspension and the efficiency of their deposition or repulsion depends on the relation between the rotational energy $U_{\text{ROT}} = \int \langle \boldsymbol{T} \rangle \, \text{d}\varphi$ or the translational energy $U_{\text{DEP}} = \int \langle \mathbf{F}_{\text{DEP}} \rangle_z \, \text{d}z$ on the one hand and the thermal energy $k_{\text{B}}T$ on the other hand.

While the torque (and the rotational energy) acting on each individual nanotube is not accessible in our experiment, we can determine the average alignment of the collectivity of nanotubes, which is a measure of U_{ROT}, in terms of the nematic order parameter S. This parameter, which is commonly used within the description of liquid crystals, is 0 for the isotropic phase with arbitrary particle orientation and 1 for the nematic phase, when all particles are aligned parallel to a common axis.[19] Since we want to compare the predicted average alignment of the nanotubes in suspension with the degree of alignment determined by absorption spectroscopy of nanotubes deposited onto a sample surface, the common axis in our case is the projection of the electric field vector during deposition onto a plane parallel to the substrate surface. For two-dimensional problems the order parameter is defined as $S = \overline{\cos(2\theta)}$ (mean value averaged over all particles), where θ is the angle between the long axis of each particle and the common alignment axis and corresponds in our case to the angle φ defined above.

To calculate S, we assume a Boltzmann distribution function for the angle φ

$$f(\varphi, U_0) = \frac{\exp(-U_0 \cos^2 \varphi / k_{\text{B}}T)}{\int_{-\pi/2}^{\pi/2} \exp(-U_0 \cos^2 \varphi / k_{\text{B}}T)\, \text{d}\varphi}$$

with U_0 defined as above. Figure 1 shows the result of our calculations assuming the following properties for the nanotubes: length $l = 0.5\ \mu$m and diameter $d = 1$ nm, depolarization factors $L_{\text{para}} = 10^{-5}$ and $L_{\text{ortho}} = 0.5$, an isotropic conductivity of both metallic and semiconducting nanotubes of $\sigma_2 = 0.35$ S/m and permittivities $\epsilon^{\text{met}}_{\text{para}} = 10^4 \epsilon_0$ and $\epsilon^{\text{met}}_{\text{ortho}} = \epsilon^{\text{semi}}_{\text{ortho,para}} = 30\ \epsilon_0$.[7,17,18] For the surfactant suspension we used $\sigma_1 = 0.1$ S/m and $\epsilon_1 = 85\epsilon_0$.

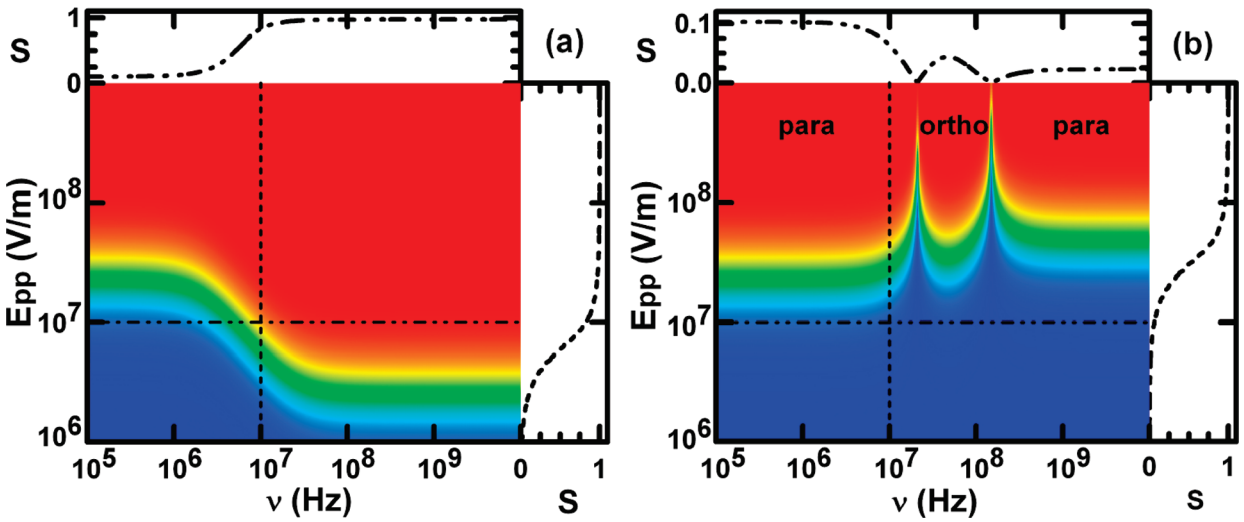

Figure 1. Nematic order parameter S as a function of the frequency ν and amplitude E_{pp} of the applied electric field. The values of S are color coded from blue (S = 0) to red ($S = 1$). Also shown are sections of the contour plot, tracing S at the frequency 10^7 Hz and electric field amplitude 10^7 V/m. The calculations are based on the structural and dielectric properties of SWNTs as given in the text. (a) Metallic nanotubes: Moderate deposition parameters lead to a high degree of alignment in the high-frequency range. (b) Semiconducting nanotubes: While the alignment at low frequencies resembles that of metallic nanotubes, the situation changes drastically for $\nu > 10^6$ Hz: much higher field strengths are necessary to overcome the random orientation and two turn-over frequencies (ν^{TO}) are predicted, which mark the transition from one stable orientation into another.

For low frequencies ($\nu < 10^6$ Hz) the conductivity dominates the polarizability and the alignment of both nanotube types is equal. For high frequencies, moderate field strengths suffice to perfectly align the metallic nanotubes. The semiconducting nanotubes, on the other hand, are randomly oriented up to much higher field strengths. Once this random orientation is overcome, the stable orientation with respect to the external field depends on the frequency. Two turn-over frequencies (ν^{TO}) mark the transitions from parallel to orthogonal and again to parallel alignment.

The samples were prepared by dielectrophoretic deposition of individually dispersed SWNTs onto an array of interdigitated Al-electrodes on a transparent quartz-glass substrate.[8] After placing a droplet of 15 μL of nanotube suspension onto the electrode array, an AC signal was applied for 10 min with a frequency $\nu = 10$ MHz and peak-to-peak voltage of $V_{pp} = 40$ V. This corresponds to an electric field E_{pp} of the order of 2×10^7 V/m, which is an order of magnitude larger than in ref 8. For high solution conductivity as in our case such large fields cause electrothermally induced motion of the liquid obstructing dielectrophoresis,[20] which is observable under a light microscope. We found that electrothermal motion can be efficiently suppressed by using AC-voltage bursts of 10−100 μs duration and 1 ms period. Moreover we observe that heat dissipation in the evolving nanotube film is greatly suppressed by the use of Al electrodes with a natural oxide layer as compared with Au electrodes. The sample was then rinsed with H_2O and gently dried off with nitrogen gas. A scanning electron micrograph of a typical sample is shown in Figure 2. The thickness of the nanotube film was determined with atomic force microscopy (AFM) to ∼ 60 nm. Supplementary Figure 2 shows an AFM image of the sample. We anticipate that the final film thickness is limited due to screening of the electric field by the nanotube film.

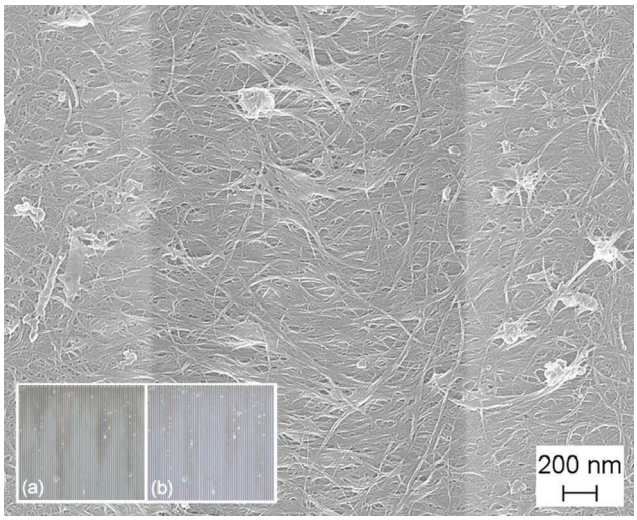

Figure 2. Scanning electron microscopy image of a SWNT film on interdigitated electrodes. The image shows a section of the sample containing one gap (dark gray area) and two half-electrodes (light gray areas), both covered completely with a thick film of dielectrophoretically deposited nanotubes. The thickness of the nanotube film is ∼60 nm, as measured with AFM. Inset shows incident-light dark-field micrographs of a larger area of a sample for two different settings of the analyzer corresponding to $\gamma = 0°$ (a) and $\gamma = 90°$ (b), as defined in Figure 3. The strong difference in contrast reflects the polarization dependent absorption of the nanotubes.

To measure the absorption spectra of our films, we used a Fourier transform infrared spectrometer (Bruker Equinox 55) combined with an infrared microscope (Bruker Hyperion 2000). Figure 3 shows a schematic of the measurement setup. Nonpolarized light from the light source passes through an aperture and illuminates the sample from the bottom. Since the electrodes are non-transparent, light passes only through the gaps and is partly absorbed by the SWNT film. By

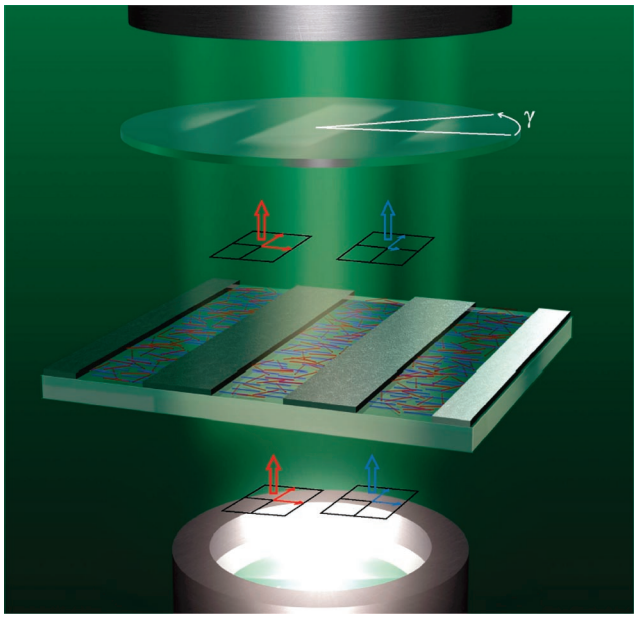

Figure 3. Schematic of the setup used for polarization dependent absorption measurements on dielectrophoretically deposited SWNTs. Nonpolarized light illuminates the sample from the bottom and is partly absorbed by the nanotube film covering the electrode gaps. An analyzer between sample and detector allows for polarization dependent measurements. While metallic nanotubes (depicted as blue rods) in the gaps are aligned parallel to the external field and hence perpendicular to the electrodes, semiconducting nanotubes (depicted as red rods) are randomly oriented. For clarity, nanotubes deposited on top of the electrodes are not included in this schematic, since they do not contribute to the absorption spectra. The anisotropic absorption by metallic SWNTs and the isotropic absorption by semiconducting SWNTs is indicated by the blue and red arrows, respectively.

varying the angle of the analyzer, which is placed between sample and detector, the polarization dependence of the absorption is determined. Due to a large depolarization effect SWNTs preferentially absorb the component of the light parallel to the nanotube axis.[21] It is therefore possible to determine the alignment of nanotubes in a sample by analyzing the polarization dependence of the absorption spectra.[22]

The black curves in Figure 4 show absorption spectra measured on the sample shown in Figure 2. The spectral range was chosen to cover the M1 absorption band of metallic SWNTs (centered around 650 nm for our nanotube material) as well as the S2 absorption band of semiconducting nanotubes (centered around 950 nm).[23] The main observation is that the shape of the S2-peak is virtually independent of the setting of the analyzer, which is characterized by the angle γ between the axis of the analyzer and the direction of the external electric field during the dielectrophoretic deposition. By contrast, the height of the M1 peak depends strongly on the analyzer setting. It is very pronounced for $\gamma = 0°$ and almost completely suppressed for $\gamma = 90°$. A similar behavior was observed in samples prepared by dielectrophoresis of SWNTs dispersed with different surfactants and length distributions but comparable deposition parameters (see Supplementary Figures 3−6).

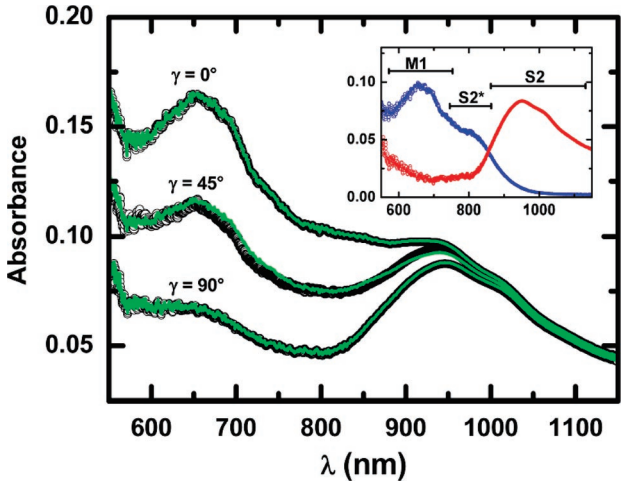

Figure 4. Absorption raw data for three settings of the analyzer (black curves). The angle γ is defined with respect to the external field during deposition. While the peak around 650 nm, which corresponds to metallic nanotubes ("M1"), strongly depends on the setting of the analyzer, the peak around 950 nm, corresponding to semiconducting nanotubes ("S2"), is virtually independent. However, there is a fraction of small-diameter semiconducting nanotubes ("S2*"), that show a similar dependence as the metallic nanotubes. Note that this "S2*" shoulder can be seen more clearly in the raw data of Supplementary Figures 3−6. Green curves: fitted data using the basic spectral data "M1/S2*" and "S2" shown in the inset and fit parameters given in the text.

Obviously the degree of alignment of metallic and semiconducting nanotubes differs greatly in our sample. Metallic nanotubes are well aligned and their preferential orientation is parallel to the electric field during the deposition process. The majority of the semiconducting nanotubes are randomly oriented, but small-diameter semiconducting nanotubes (with S2 shifted to $\sim$ 800 nm, see ref 23) show an alignment similar to the metallic nanotubes. There are two important conclusions to be drawn from this analysis: (1) the SWNTs are deposited individually, not in bundles; (2) although both nanotube types apparently undergo positive dielectrophoresis for the chosen experimental conditions, their response to the external electric field is different, compatible with the theoretical considerations above. Furthermore, we performed Raman spectroscopy, that confirm the incisively different degree of alignment of the two nanotube types (see Supplementary Figures 7 and 8).

To analyze the measured absorption spectra, we first extract two sets of basic spectral data, one of them describing the absorption of the aligned nanotubes, the other one representing the randomly oriented nanotubes. The first set of data, corresponding to "M1/S2*" in the inset of Figure 4, is obtained by subtracting the data of the measurement with $\gamma = 90°$ from the measurement with $\gamma = 0°$, thereby eliminating the polarization independent contributions. To generate the basic spectrum of the randomly oriented nanotubes ("S2"), we cannot use the plain data of the 0° measurement, because there is obviously some contribution between 600 and 800 nm from the aligned nanotubes. Therefore we modify the data of the 0° measurement by subtracting a fraction of the M1/S2* data, until we obtain a flat background between 600 and 800 nm.

With this choice of basic spectra the absorbance A for a specific angle γ is given by the function[24]

$$A(\gamma) = \frac{1}{\int_{-\pi/2}^{\pi/2} \cos^2(\varphi - \gamma)\, d\varphi} \cdot \int_{-\pi/2}^{\pi/2} [A_{M1/S2^*} f(\varphi, U_0^{M1/S2^*}) + A_{S2} f(\varphi, U_0^{S2})] \cos^2(\varphi - \gamma)\, d\varphi$$

A large value of U_0 then corresponds to a narrow angular distribution, while a small value matches a wide angular distribution. The green curves shown in Figure 4 were obtained using for the "M1/S2*" tubes a value of $U_0^{M1/S2^*}/k_BT = 2.3$ and for the "S2" nanotubes a value of $U_0^{S2}/k_BT = 0$. The values for U_0 are consistent with our model calculations for SWNTs close to the substrate surface ($\sim 1\ \mu$m). This self-consistency as well as the excellent agreement of the fit with the measured data justifies the procedure for constructing the "S2" spectrum.

The different forms of alignment of metallic and semiconducting nanotubes strongly affect the determination of the composition of samples by optical absorption spectroscopy. A simple comparison of the peak heights or the peak area measured with nonpolarized light will not render the correct result, since the amount of metallic nanotubes will be underestimated. For instance, even if aligned nanotubes would absorb all parallel polarized light, the absorbance measured with nonpolarized light could never exceed 0.3. The fitting procedure described above depends strongly on the choice of the basic spectra and is therefore not appropriate for a quantitative analysis of the sample composition.

A point we have not discussed so far is why the alignment of small-diameter semiconducting nanotubes "S2*" resembles that of metallic nanotubes "M1". As we assume the conductivity σ_2 of all nanotubes to be dominated by the surface conductance κ, a smaller nanotube diameter d results in a bigger value of $\sigma_2 \propto \kappa/d$ [25,26,7] and therefore a larger value of U_0, which increases the alignment. Another possible explanation would be a diameter-selective dispersion of the nanotubes in the surfactant, which allows for residual bundles of small-diameter semiconducting nanotubes with metallic nanotubes. A comparison of fluorescence maps of nanotubes dispersed in SDS (sodium dodecyl sulfate) and SDBS indeed suggests such selectivity in the case of SDBS.[23] Further analysis is necessary to verify either of these interpretations.

We now discuss the prediction of our nanotube DEP model, that within a certain frequency range, $\nu_1^{TO} \ldots \nu_{ortho}^{CO}$, a deposition of semiconducting nanotubes can occur due to their perpendicular polarizability and that this effect should only be observable in experiments at very large electric fields. In earlier experiments under moderate fields ($E_{pp} = 20\ V_{pp}/20\ \mu$m) semiconducting SWNTs were not deposited above the critical frequency $\nu_c \sim 3$ MHz.[6,7] In a recent experiment at larger fields ($10\ V_{pp}/2\ \mu$m) we observed $\nu_c \sim 30$ MHz.[8] Finally, in this work we find at very large electric fields ($40\ V_{pp}/2\ \mu$m) $\nu_c > 80$ MHz (see Supplementary Figures 4−7). This agrees with the model that at moderate fields the probed critical frequency is due to the parallel polarizability (ν_{para}^{MW}), whereas at larger fields and frequencies it is the orthogonal polarizability that progressively dominates the dielectrophoresis. To demonstrate this situation, we present numerical field simulations, for which the finite element solver FlexPDE was used.[27]

The dielectric force is defined within the particle's coordinate system as $\boldsymbol{F}_{DEP} = (1/2)\nabla(\alpha_{para}\boldsymbol{E}_{para}^2 + \alpha_{ortho}\boldsymbol{E}_{ortho}^2)$. As a means of simplification, we assume a fixed orientation of the nanotubes with respect to the global coordinate system. We can then easily transform from the particle's coordinate system into the global coordinate system: for horizontally aligned nanotubes we derive $\boldsymbol{F}_{DEP} = (1/2)(\alpha_{para}\nabla E_x^2 + \alpha_{ortho}\nabla E_z^2)$ and for vertically aligned nanotubes $\boldsymbol{F}_{DEP} = (1/2)(\alpha_{para}\nabla E_z^2 + \alpha_{ortho}\nabla E_x^2)$.

Figure 5 shows the simulated dielectric force fields acting on metallic (a and b) and semiconducting nanotubes (c and d) assuming horizontal or vertical alignment of the nanotubes as indicated. We chose a representative field frequency of 50 MHz such that α_{para}^{met}, α_{ortho}^{met}, and $\alpha_{ortho}^{semi} > 0$ and $\alpha_{para}^{semi} < 0$. Note that metallic nanotubes are well aligned along the electric field lines, as shown before. Since the electric field lines are horizontal above the gap, Figure 5a applies to metallic nanotubes in this region, whereas Figure 5b applies to metallic nanotubes above the electrode, where the field lines are vertical. Therefore, metallic nanotubes always experience an attractive force toward the substrate. The orientation of semiconducting nanotubes on the other hand is random under the chosen conditions. Comparing the two representative situations of horizontal and vertical alignment, a dramatic change in the force fields is observable. Taking a closer look at Figure 5c, we see that the forces are repulsive in regions where the nanotubes are parallel to the electric field (above the gaps), while they are attractive when the nanotubes are orthogonal to the electric field (above the electrodes). The same, of course, holds true for Figure 5d. These simulations clearly show that semiconducting nanotubes can be attracted to the substrate surface due to their orthogonal polarizability, albeit the magnitude of the force is smaller than in the case of the metallic nanotubes. With respect to the measured random orientation of semiconducting SWNTs in the gap, we note that the DEP force field simulations predict repulsion only for semiconducting nanotubes which are oriented along the *x*-axis. Nanotubes oriented along the *y*-axis and *z*-axis are attracted, which should result in a depletion of semiconducting nanotubes close to $\gamma = 0$. However, considering the drag coefficient of nanotubes, which depends on the angle between the nanotube axis and the direction of motion,[28] we expect the highest deposition rate for vertically oriented semiconducting nanotubes, which upon touching the surface flip over without preferential direction.

The efficiency of the nanotube deposition depends on the relation U_{DEP}/k_BT. Figure 6 shows this relation for semiconducting nanotubes for different field strengths E_{pp} as function of the field frequency ν, with the translational energy split into a part depending on α_{para} and another depending on α_{ortho}. We can clearly make out frequency domains, where the attraction due to the orthogonal polarizability prevails over the repulsion due to the parallel polarizability. This effect is

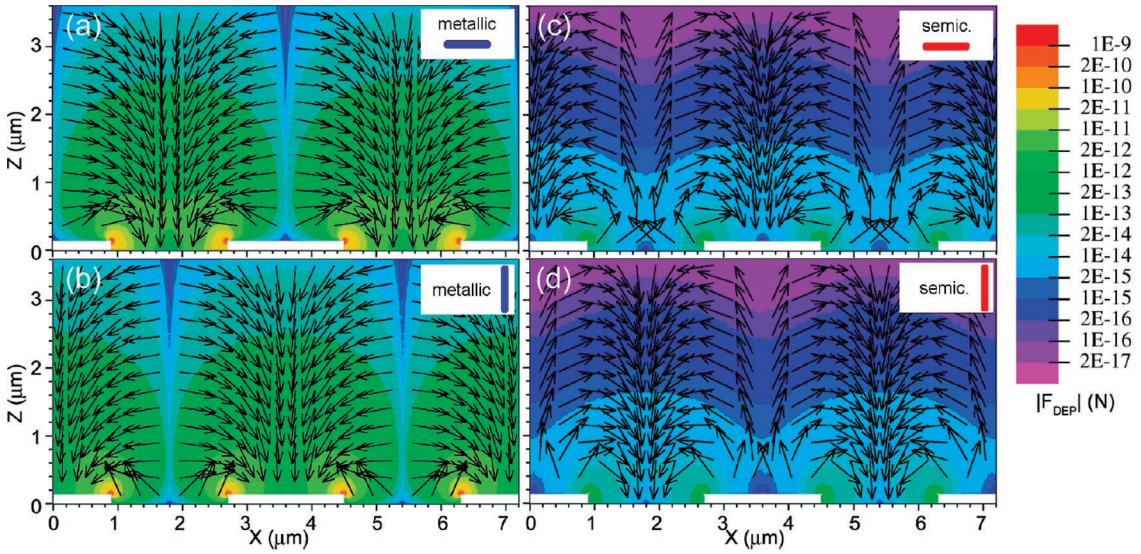

Figure 5. Simulation of the dielectrophoretic force fields. For the simulation we choose a representative section extending from the center of a positively charged electrode to the center of the next positively charged electrode. This "unit cell" then contains two electrodes and two gaps on top of a 50 μm thick quartz substrate with permittivity $\epsilon = 5\epsilon_0$ and below a 50 μm thick aqueous layer with $\epsilon = 85\epsilon_0$. The frequency of 50 MHz was chosen such that α_{para}^{met}, α_{ortho}^{met}, and $\alpha_{ortho}^{semi} > 0$ and $\alpha_{para}^{semi} < 0$. The calculations are based on the structural and dielectric properties of SWNTs as given in the text. (a and b) $\boldsymbol{F}_{DEP}$ for metallic nanotubes and (c and d) $\boldsymbol{F}_{DEP}$ for semiconducting nanotubes, assuming the nanotubes to be horizontally aligned or vertically aligned as indicated. While metallic nanotubes are attracted toward the substrate surface, semiconducting nanotubes experience either attractive or repulsive forces depending on their orientation with respect to the electric field.

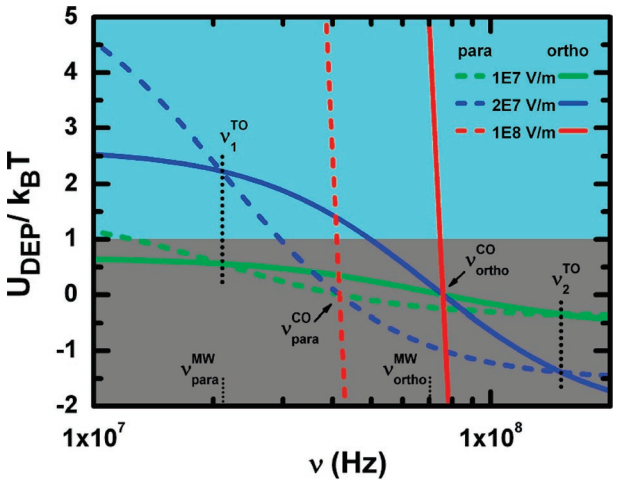

Figure 6. Standardized DEP potential U_{DEP}/k_BT for semiconducting nanotubes as a function of the frequency ν of the applied electric field calculated for various field strengths E_{pp}. The calculations are based on the structural and dielectric properties for semiconducting SWNTs as given in the text. The nanotubes are deposited only when $U_{DEP}/k_BT > 1$ (highlighted in cyan). The indices "para" and "ortho" characterize the orientation of the nanotubes with respect to the electric field. The frequencies marked are the turnover frequencies (ν^{TO}, as defined in the text), the frequencies corresponding to Maxwell−Wagner relaxations (ν^{MW}) and the crossover frequencies (ν^{CO}), where the Clausius-Mosotti factor changes its sign.

more pronounced for high field strengths. The frequency at which $(U_{DEP}/k_BT)_{ortho}$ becomes larger than $(U_{DEP}/k_BT)_{para}$ depends critically on the assumed values for the conductivity and the permittivity of nanotubes and suspension. For our chosen set of parameters, it is slightly larger than the experimentally observed value.

All these observations have to be considered when using DEP under very large electric fields, for example in nanotube separation, and some of the contradictory results in literature might be attributed to the critical dependence of the nanotube dielectrophoresis on the electric field strength and frequency.[9,29] Note that for different experimental setups the field amplitude at the electrode tips can significantly differ from the nominal amplitude due to capacitive coupling or impedance mismatch.

The results show that the model of nanotube dielectrophoresis, which has been used so far and is based on a scalar dependence of the polarizability of the external field, is not sufficient to describe SWNTs due to their structural and dielectric anisotropy. Within an advanced model that also incorporates contributions from the polarizability orthogonal to the nanotube axis, we predict a strikingly different alignment behavior of metallic and semiconducting nanotubes under the influence of an electric field and a possible deposition of semiconducting nanotubes for frequencies above the crossover frequencies defined before due to the orthogonal polarizability for very large electric fields. Our polarization-dependent measurements of the optical absorption on films of dielectrophoretically deposited carbon nanotubes give clear evidence for the high degree of alignment of the metallic nanotubes and a random orientation of the semiconducting nanotubes, as predicted. Additionally, we have illustrated the decisive influence of the orthogonal polarizability onto the dielectric force acting on semiconducting nanotubes by means of finite-element simulations.

Acknowledgment. The authors thank M. Pimenta and L. M. Malard for performing Raman measurements, C. Becker for assistance with the absorption measurement, and B. Schmidt for discussions. S.B. and R.K. acknowledge funding by the Initiative and Networking Fund of the

Helmholtz-Gemeinschaft Deutscher Forschungszentren (HGF) and A.V. acknowledges the Alexander von Humboldt Foundation.

Supporting Information Available: Text giving experimental details and Supplementary Figures 1−8, showing an optical spectrum (1), atomic force microscope image (2), polarization dependent absorption spectra (3−6), and Raman spectra (7 and 8). This material is available free of charge via the Internet at http://pubs.acs.org.

References

(1) Pohl, H. A. *Dielectrophoresis*; Cambridge University Press: London, 1978.
(2) Krupke, R.; Hennrich, F.; Weber, H. B.; Beckmann, D.; Hampe, O.; Malik, S.; Kappes, M. M.; v. Löhneysen, H. *Appl. Phys. A: Mater. Sci. Process* **2003**, *76*, 397−400.
(3) Krupke, R.; Hennrich, F.; Weber, H. B.; Kappes, M. M.; v. Löhneysen, H. *Nano Lett.* **2003**, *3*, 1019−1023.
(4) Dong, L.; Bush, J.; Chirayos, V.; Solanki, R.; Jiao, J.; Ono, Y.; Conley, J. F.; Ulrich, B. D. *Nano Lett.* **2005**, *5*, 2112−2115.
(5) Lee, S. W.; Lee, D. S.; Yu, H. Y.; Campbell, E. E. B.; Park, Y. W. *Appl. Phys. A: Mater. Sci. Process* **2004**, *78*, 283−286.
(6) Krupke, R.; Hennrich, F.; v. Löhneysen, H.; Kappes, M. M. *Science* **2003**, *301*, 344−347.
(7) Krupke, R.; Hennrich, F.; Kappes, M. M.; v. Löhneysen, H. *Nano Lett.* **2004**, *4*, 1395−1399.
(8) Krupke, R.; Linden, S.; Rapp, M.; Hennrich, F. *Adv. Mater.* **2006**, *18*, 1468−1470 (Errata: The applied peak to peak voltage was 10 V, instead of 20 V as stated in the text).
(9) Baik, S.; Usrey, M.; Rotkina, L.; Strano, M. J. *Phys. Chem. B* **2004**, *108*, 15560−15564.
(10) Peng, H.; Alvarez, N. T.; Kittrell, C.; Hauge, R. H.; Schmidt, H. K. *J. Am. Chem. Soc*. **2006**, *128*, 8396−8397.
(11) Lee, D. S.; Kim, D. W.; Kim, H. S.; Lee, S. W.; Jhang, S. H.; Park, Y. W.; Campbell, E. E. B. *Appl. Phys. A: Mater. Sci. Process* **2005**, *80*, 5−8.
(12) Dimaki, M.; Bøggild, P. *Nanotechnology* **2004**, *15*, 1095−1102.
(13) Rosales, C.; Lim, K. M. *Electrophoresis* **2005**, *26*, 2057−2065.
(14) Jones, T. B. *Electromechanics of Particles*; Cambridge University Press: Cambridge, U.K., 1995.
(15) Schnakenberg, J. *Elektrodynamik*; Wiley-VCH: Berlin, 2003.
(16) Levy, O. *Phys. Rev. E* **2002**, *66*, 011404.
(17) Benedict, L. X.; Louie, S. G.; Cohen, M. L. *Phys. Rev. B* **1995**, *52*, 8541−8549.
(18) Kozinsky, B.; Marzari, N. *Phys. Rev. Lett*. **2006**, *96*, 166801.
(19) Chaikin, P. M.; Lubensky, T. C. *Principles of condensed matter physics*; Cambridge University Press: Cambridge, U.K., 1995.
(20) Castellanos, A.; Ramos, A.; González, A.; Green, N. G.; Morgan, H. *J. Phys. D: Appl. Phys.* **2003**, *36*, 2584−2597.
(21) Ajiki, H.; Ando, T. *Physica B* **1994**, *201*, 349−352.
(22) Islam, M. F.; Milkie, D. E.; Kane, C. L.; Yodh, A. G.; Kikkawa, J. M. *Phys. Rev. Lett.* **2004**, *93*, 037404.
(23) Lebedkin, S.; Arnold, K.; Hennrich, F.; Krupke, R.; Renker, B.; Kappes, M. M. *New J. Phys.* **2003**, *5*, 140.
(24) Gommans, H. H.; Alldredge, J. W.; Tashiro, H.; Park, J.; Magnuson, J.; Rinzler, A. G. *J. Appl. Phys.* **2000**, *88*, 2509−2514.
(25) Morgan, H.; Green, N. G. *J. Electrostatics* **1997**, *42*, 279−293.
(26) Hughes, M. P. *J. Colloid Interface Sci.* **2002**, *250*, 291−294.
(27) http://www.pdesolutions.com
(28) Walther, J. H.; Werder, T.; Jaffe, R. L.; Koumoutsakos, P. *Phys. Rev. E* **2004**, *69*, 062201.
(29) Krupke, R.; Hennrich, F. *J. Phys. Chem. B* **2005**, *109*, 17014−17015.

NL0706751